Thin polymeric CuO film from EPD designed for low temperature photothermal absorbers

S. Shehayeb, Xavier Deschanels, J. Lautru, L. Ghannam, Michaël Odorico, I. Karame, G. Toquer

Thin polymeric CuO film from EPD designed for low temperature photothermal absorbers

S. Shehayeb[a,b], X. Deschanels[a], J. Lautru[a], L. Ghannam[b],

M. Odorico[a], I. Karamé[b], G. Toquer[a,*]

a. Institut de Chimie Séparative de Marcoule - UMR 5257, CEA, CNRS, ENSCM, Univ Montpellier, Marcoule, France

b. Laboratory of Catalysis, Organometallic and Materials (LCOM), Faculty of Sciences I, Lebanese University, Hadath, Lebanon

Keywords: Nanoparticles; Electrophoretic deposition; selective tandem materials; Selective solar absorbers CuO; PEI

guillaume.toquer@enscm.fr

Abstract

The creation of a tandem solar absorber based on highly UV-Vis-NIR absorbing nanofilm deposited onto a highly IR reflecting platinized silicon wafers is processed through electrophoretic deposition (EPD). The stabilization of a CuO colloidal aqueous suspension is first studied by adding polyethyleneimine (PEI) as cationic polymer acting both as charging agent and as electro-steric stabilizer. The colloidal stability as a function of the suspension pH is investigated prior to EPD, by Laser Doppler Velocimetry and atomic force microscopy. Tandem absorbers are obtained by varying different EPD parameters to control the thickness and the morphology of the film, in order to tune and optimize the final optical properties. The deposition thickness is then compared relative to the applied potential difference and deposition time range. The morphology of the deposits and the thickness of the coatings are analysed by scanning electron microscopy (SEM). The density is obtained from energy-dispersive X-ray spectroscopy (EDX) using X-film software, Total Organic Carbon (TOC) and Hamaker equation. CuO tandem absorbers are found to possess a high density with homogeneous and crack-free surfaces. Finally, absorptance (α) and emittance (ε) are calculated from the reflectance spectra of the UV-Vis-NIR and the Fourier Transform Infra-Red (FTIR) spectroscopy respectively. These latter values are combined to determine the efficiency (η) of the tandem material.

1. Introduction

In order to limit the use of fossil fuels, the production of hot water by using tandem photothermal collectors is in growing importance. The efficiency of the absorber is determined by its high optical selectivity by having a high absorptance α (*i.e.* low reflectance) over the spectral range of solar emission (0.5-2.5 µm) and a low emittance ε (*i.e.* high reflectance) in the mid and far infrared region (2.5-20 µm). These two properties can be achieved by forming tandem absorber composed of highly absorbing UV-VIS and NIR layer deposited on a highly IR reflecting metallic substrate. The absorption of the upper layer could be a result of the intrinsic properties of the material (*e.g.* black paint) or due to texturing created by the processing technique that shift the absorption edge toward higher wavelengths [1]. In the 20th century, selective surfaces of absorber/ reflector tandems were metal-oxide and sulfide layers coated onto various metals. Metal oxides of Copper, Chromium, Zinc and Nickel were generally used. These layers have showed high selectivity (α/ε) by having α>0.9 and a low ε. Non-selective layers like black paints have high α (>0.9) and very high ε (>0.9).

In this context, copper oxides present interesting optical properties (*i.e.* intrinsic selectivity) for the design of photothermal absorbers [2]. It has already been obtained by several processes including reactive sputtering [3], chemical vapor deposition (CVD) [4], chemical conversion [5], thermal oxidization [6] [7], chemical conversion [8], cathodic arc deposition [9] and DC co-sputtering of Cu and Al [10]. The increase of the selectivity is induced by optical trapping of energy or wavelength discrimination by surface roughening and/or even with the formation of dendritic structure. Such structures absorb efficiently high energy solar radiation from multiple absorption and reflection, and in the thermal infrared region the wavelengths of the radiation are now much larger than the dendrite spacing, while the emittance in the IR spectral region is rather unaffected since the relevant wavelengths are much larger than the dendrite, and consequently the surface appears at this scale fairly smooth [11] [12].

In this work, from an electrophoretic deposition (EPD) based on dispersed CuO nanoparticles, we have attempted to adjust the coating thickness and structure, having a favorable surface in order to optimize the optical efficiency. Compared to the above used methods, electrophoretic deposition (EPD) is fairly rapid and economic. It is based on a two-step deposition process. In the first step (electrophoresis), charged particles suspended in a suitable

medium are forced to migrate upon the application of an electric field. In the second step (deposition), particles form a coherent deposit on the electrode to which they are attracted. The required coating is obtained while operating at room temperature compared to CVD and PVD techniques (cathodic arc deposition and DC sputtering) where high processing temperature is required. Compared to chemical, thermal conversion and dip coating methods, there is not some thermochemical post deposition steps with EPD, and then the bulk properties of the starting material are conserved. By EPD, the content, density and the homogeneity of the coating are expected to be tuned by varying process and suspension parameters. Although, EPD coating is concentration dependent, an initial suspension concentration as low as 0.05 wt% is sufficient in order to form a coating. This makes EPD economic compared to the other wet deposition techniques. Up to now several studies have reported successful CuO dispersion [13] using catechol derivatives (such as Tiron) [14], Poly(vinyl alcohol) [15], PEG [16] in water. Nevertheless, none of these was dedicated to a charged suspension of CuO suitable for EPD or for the study of the stabilization of CuO nano-powder. The strategy of coating or grafting polymer to the surface of nanoparticles is often used to avoid their aggregation by inducing surface-surface repulsion [17] [18]. Polyethyleneimine (PEI) is a cationic dispersant widely used in different sizes and structures for the preparation of stable suspensions of Ti nanoparticles [13], Ti_3SiC_2 [19], TiN [20], $BaTiO_3$ [21], ZnO [22]. The amine groups complex the surface of the metal oxide through dative bonds while the other free amine groups are pH sensitive and readily adsorb protons in aqueous solution which in turn should affects the mechanism of stabilization resulting mainly in electro-steric stabilization of CuO nanoparticles [23] [24]. In addition, PEI also plays the role of binder in the final film by avoiding crack formation during the drying process.

We also investigate the stabilization of CuO in water by using PEI in order to form CuO thin films by EPD. Firstly, the suspension parameters are adjusted by varying the concentration of the polymer and then the pH of the suspension. Secondly, the EPD processing parameters (applied electric field and deposition time) were adjusted in order to control the structure (density, roughness, thickness) and consequently the optical efficiency of the deposit. This colloidal route offers the advantage of the formation of the CuO film from a bottom-up approach controlling the roughness and the structure of the film.

2. Experimental section

2.1. Preparation of the CuO/PEI suspension

Suspensions of 0.88 wt % PEI (M_W~2000 g mol^{-1}, 50 wt % in H_2O, from Sigma Aldrich) in distilled water, were stirred for 30 mins then few drops of 1.5M HNO_3 were used to attain the wished pH. Then 0.05 wt% of CuO nanoparticles (<50nm, Sigma Aldrich) were added to each suspension and left to stir for 2 days.

2.2. Characterization of the CuO/PEI suspension

In order to follow the stabilization nanoparticles by PEI at different pH, the charge of the suspended nanoparticles was determined *via* the electrophoretic mobility measured by laser Doppler velocimetry (zetasizerNanoZS, Malvern). The zetasizer uses electrophoresis to determine the electrophoretic mobility which is simply related to zeta potential through the Henry equation by using the Smolukowski model.

Besides, the stabilization of nanoparticles was also studied by atomic force microscopy (AFM), the suspension of 0.05 wt% CuO was diluted 100 folds, and a drop was placed on a freshly cleaved “Mica” disc for each pH. Mica substrates provide a flat and even surface for high resolution AFM.

2.3. EPD procedure

Electrophoretic experiments are conducted in potentiostatic conditions using a VersaSTAT 4 potentiostat controlled by the Versastudio software (Princeton Applied Research®), based on three connection electrodes: the working electrode (WE) at 1 cm from the counter electrode (CE) and the reference (RE) electrode (Ag/AgCl filled with 3M KCl solution 0.2 V/SHE), placed in between. The WE and the CE received as platinum coated silicon wafers discs (from Sil’tronix®), were cut into 15x20 mm^2 rectangles. The EPD instrument supplies absolute compliance voltage of 12 V at full rated current. The software yields electrochemical cell features (current, resistance, time, apparent applied potential difference). Before each EPD

experiment, both WE, CE and RE were dipped in the PEI/CuO suspension prepared. After EPD, the working electrode was then removed and dipped 2 times in a beaker containing water and then in one containing ethanol. Finally, the deposit was left to dry vertically, in a closed box, for two days at room temperature before further analysis.

2.4. Spectral reflectance characterization

Low temperature tandem solar absorbers are characterized by solar absorptance (α), thermal emittance (ε) and efficiency (η). The α value of a surface may be defined as the weighted fraction (by total power density) of the absorbed radiation to that incident on the surface, given by:

$$\alpha = \frac{\int_{0.28}^{2.5} I_{solar}(\lambda)[1 - R(\lambda)]\, d\lambda}{\int_{0.28}^{2.5} I_{solar}(\lambda)\, d\lambda} \qquad \text{(Equation 1)}$$

Where $R(\lambda)$ is the spectral reflectance of the surface and $I_{solar}(\lambda)$ is the normal spectral irradiance, defined by the ISO standard 9845-1 (1992) for air mass (AM) 1.5. The equation 4 completely describes the collection ability of the material over a given wavelength range, without any consideration given to the losses due to thermal emittance, hence the lower and the upper limit of the integration are that of the solar spectrum between 0.28 and 2.5 μm, respectively. The ε value of a surface is defined from the weighted fraction (by total power density) of the emitted radiation at a particular temperature to the spectral Planck radiation, $\rho(\lambda)$ at the same temperature than the surface and established as:

$$\varepsilon = \frac{\int_{2.5}^{16} I_{blackbody}(\lambda, T)[1 - R(\lambda)]\ d\lambda}{\int_{2.5}^{16} I_{blackbody}(\lambda, T)\, d\lambda} \qquad \text{(Equation 2)}$$

The simplified heat balance of a solar collector combines α and ε by the following expression:

$$Q_u = S_c.\alpha.E_s - S_a.\varepsilon.\sigma(T_a^4 - T_0^4) - S_a.H.(T_a - T_0) \qquad \text{(Equation 3)}$$

Where Q_u is the useful energy, S_c the collector's surface (m^2), S_a the absorber surface (m^2), H the thermal losses coefficient by conduction and convection (W. m^{-2}. K^{-1}), E_s the solar radiation flux W. m^{-2}, σ the Stefan–Boltzmann constant (W. m^{-2}. K^{-4}), T_a the temperature of the

absorber (K), T_0 the temperature of the environment (K). If one considers only the optical losses, *i.e.* the heat losses by conduction and convection are neglected, an efficiency η of the collector is defined having the following expression:

$$\eta = \alpha - \frac{\varepsilon}{XE_s}\sigma(T_a^4 - T_o^4) \qquad \text{(Equation 4)}$$

Where $X = \frac{S_c}{S_a}$, the factor of concentration is considered equal to 1 (being exposed to direct solar radiation). At a fixed operation temperature, this measure probes the efficiency of the absorber. Thus, one can conclude that it increases by the increasing of α value or by the diminishing of ε value. Ideal cases are obtained when α approaches 1 and ε approaches 0.

2.5. Energy Dispersive X-Ray spectroscopy

The determination of thin film thickness and density are established by using Energy Dispersive X-Ray (EDX) coupled with X-film® software. Conventional measurements are performed at varying incident electron energy (in the 5-30 keV range) which allows the variation of the depth of penetration into the material resulting in different k-ratios. These k-ratios are processed with the help of thin-film analysis software (*i.e.* X-film®) which determines the density and thickness by fitting the predictions of an X-Ray emission model to the measured k-ratios. The obtained expression from the software is in the form of "ρz (mg cm^{-2})". Then from the measured experimental value of thickness z (μm) obtained *via* SEM cross-section observations, the density ρ (g cm^{-3}) is finally determined.

3. Results and Discussion

3.1. Colloidal Suspension

The PEI used in these experiments is a highly branched polyamine, composed of primary, secondary and tertiary amines achieving their cationicity through their protonation from the surrounding medium. However, primary amine groups which are the chain terminating units are the most basic and reactive. The ionization pH range of low M_W branched PEI used is between pH=2-10 [21].

In a first step before EPD process, to study the effect of pH at the zeta potential value (ζ (mV)), 0.05 wt % of CuO were added to 0.88 wt % PEI at pH working range of 3, 6, 9, and 11. The addition of CuO to PEI solution resulted in blue solution which has UV-VIS absorption band maxima at ~270 nm and ~640 nm showing the formation of dative bond or a complex

between surface Cu^{2+} of CuO nanoparticles and amine groups of PEI [23] [24].The corresponding ζ of CuO/PEI system as a function of pH are presented in Fig. 1. The measured ζ of PEI is positive for the whole pH range studied (3-11). The magnitude of the ζ increases with decreasing pH ranging between ~4 and 22 mV. Upon the addition of CuO, the ζ shifts to higher positive values varying between 5 mV for pH=11 and 35 mV for pH=3. This proves that the PEI is well adsorbed on the surface of CuO and repulsive forces are dominating. The low values obtained at pH=11 are due to the fact that PEI is not enough protonated. At pH=9, the corresponding ζ (24 mV) proves a build-up of charge and the existence of a dative bond. At pH=3 the highest ζ (+35 mV) is obtained. This shows that the interaction between PEI and CuO is due to the dative bonds formed between Cu(II) surfaces and the amino groups of PEI resulting in surface complexation of CuO. While the other free amino groups play the role of charging agents which explain the increase of ζ with decreasing pH.

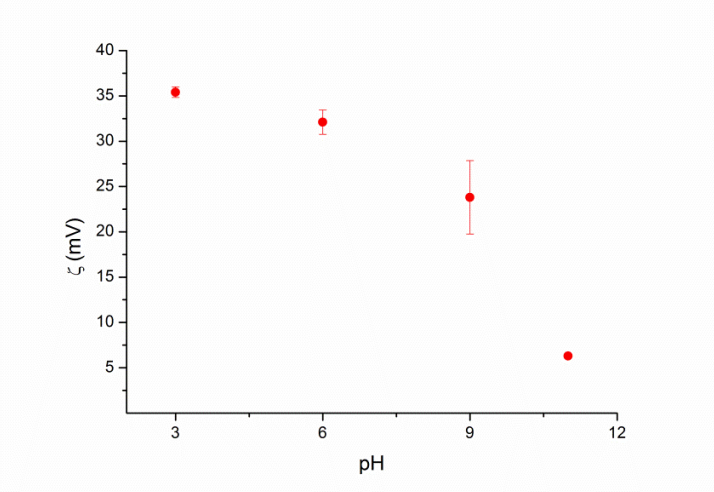

Figure 1: ζ (mV) of CuO/PEI (0.05 wt % CuO/ 0.88 wt% PEI) suspension as a function of pH.

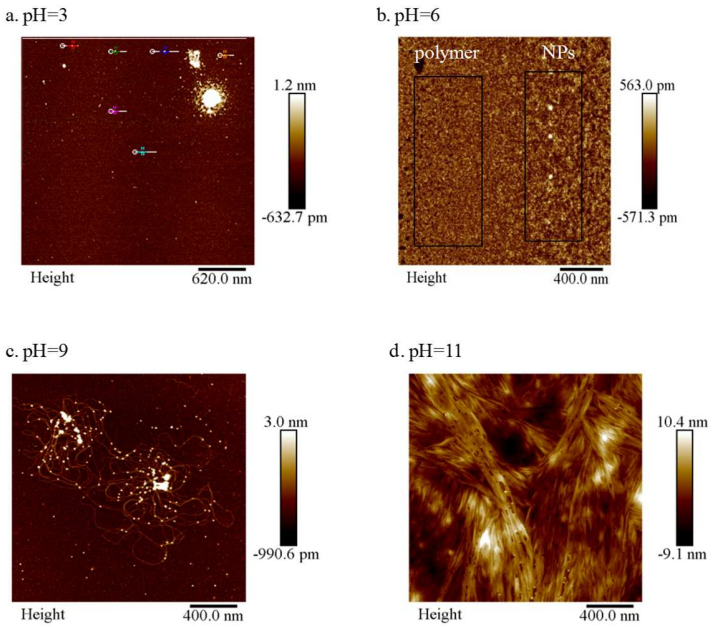

Figure 2: AFM images at pH=3 (a), pH=6 (b), pH=9 (c) and pH=11 (d).

The AFM study of the suspensions studied at different pH is presented in Fig. 2. The results obtained from AFM and laser Doppler velocimetry are consistent. The high zeta potential obtained at pH=3 is due to high repulsive forces between individually charged polymers and between polymers and nanoparticles. Nanoparticles are found to be surrounded by polymer on one hand and polymers are found individually. These repulsive interactions due to the full protonation lead to their subsequent stabilization. At pH=6 the stabilization of nanoparticles by PEI is not evident since upon drying of the drop, nanoparticles and polymer chains are observed separated. At pH=9, nanoparticles show higher interaction with the polymer chains and are found connecting polymers together. Finally, at pH=11 a denser network of polymers and nanoparticles is observed. Polymers are adsorbed on the surface of CuO nanoparticles through the uncharged amine groups. The low ionization of PEI at this pH explains the low ζ value as well. The best stabilization conditions are at pH=3 and pH=9. At both pHs, the mechanism of stabilization could be described as electro-steric repulsion. As a conclusion, at pH=3 fully protonated amine groups [-$(NH_3)^+$] of the polymer repels other similar groups and un-protonated amine groups form weak dative bonds with the surface Cu^{2+}. The former prevents the agglomeration of CuO while the latter maintains the stability of the suspension and prevents the sedimentation of CuO. At pH=9 stronger dative bonds are formed between the surface of Cu^{2+} and the amine groups. The slight protonation results in inter-repulsion between of the protonated amine groups in the

polymer chain. CuO nanoparticles surrounded by polymer are expected to be found in the suspension at pH=9 while at pH=3 individual protonated polymers will more probably exist and deposit alone during cathodic EPD.

3.2 Electrophoretic deposition (EPD)

3.2.1. Thickness of the coating

The yield of EPD depends directly on the charge of the suspended NPs. Thus, the thickness of the deposit obtained should be proportional to ζ value. From the SEM cross-section micrographs of the deposits obtained at different pH, the thickness is measured between 1358±33 nm for deposits obtained at pH=11 up to 1627±44 nm for deposits obtained at pH=3 (see Fig. 3). A linear relationship between pH and thickness of the deposit is observed here and the deposit thickness increases with decreasing pH and increasing ζ.

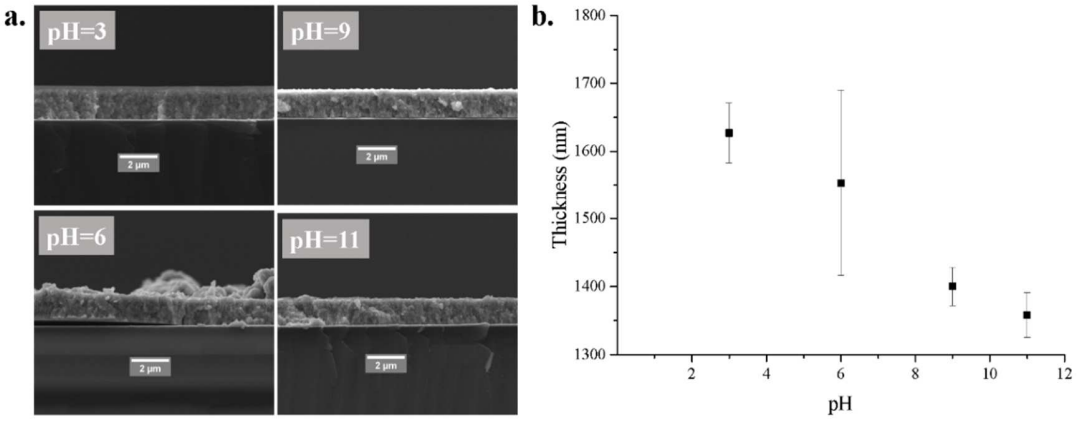

Figure 3: SEM cross-sections (a) of CuO/PEI deposits at pH= 3, 6, 9 and 11 for E=2V cm^{-1} and t=120 min and corresponding measured thickness versus pH (b).

Electrolysis reactions usually affect the morphology of the deposit by the formation of gas bubbles, during EPD, leading to the incorporation of empty holes/spaces into the final coating [25]. As H^+ ions increase in solution, H_2 gas formation increases at the cathode and thus more bubble are incorporated as holes in the deposit. This activity could be observed in the SEM micrograph of the coating obtained at pH =3 (see Fig. 4). For pH=9, we found that the deposit obtained is more homogeneous and no empty gas holes/spaces are present, compared to pH=3. At pH=11, the deposition of large agglomerates is observed, which is expected, since the

nanoparticles are not sufficiently charged having the lowest ζ value (6.3 ± 0.2 mV). Thus, large charged agglomerates migrate to form the deposit, resulting in reduced homogeneity and uniformity.

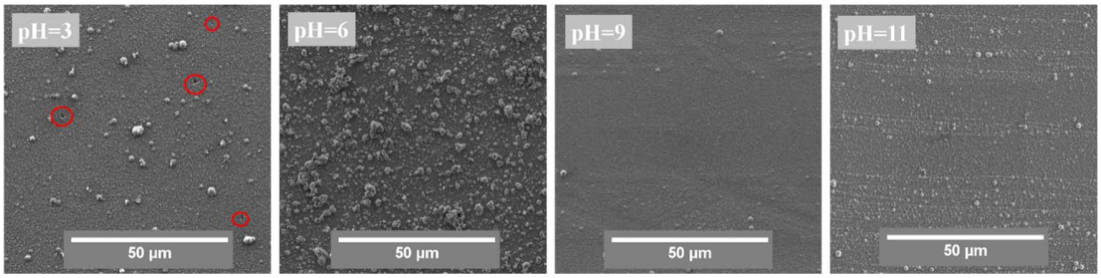

Figure 4: Top-view SEM micrographs of EPD deposit of CuO/PEI obtained at pH=3. Holes generated from electrolysis reaction are shown in red.

3.2.2. Density of the coatings

Fig. 5 shows the calculated density (ρ_{theo}) based on the estimated volume percentage (%V) of PEI in the deposit obtained from the total organic carbon (TOC) at different pH, compared with the experimental density ($\rho_{X\text{-}film}$). For the same applied electric field of 2V cm^{-1} and deposition time of 120 min, the %V of polymer present in the deposit obtained decreases with the pH from 32 % at pH=3 down to ~20% at pH=11. However, the calculated density of the film increases with the pH reaching its highest value at pH=9 being 5.41 g cm^{-3}. These values are calculated by considering bulk density ρ and volume fraction of the polymer and that of the CuO (*e.g.* at pH=9: ρ(theoretical)= ρ_{CuO} x V_{CuO} + ρ_{PEI} x V_{PEI}= (6.3x0.83 + 1.08x0.17) = 5.41g cm^{-3}). The real/experimental density of the deposits from X-film is 5.02 and 5.90 g cm^{-3} for pH=3 and pH=9, respectively. Both experimental and theoretical density values are close in magnitude. The slightly higher value obtained with X-film is expected, since the presence of Cu metal (ρ=8.96g cm^{-3}) is not quantified and only the density of CuO is taken into account which is lower than that of Cu. Thus, a general lowering in the calculated density value is expected. As a result, the density of CuO coatings obtained for E=2V cm^{-1} at pH=9 is much higher than 5 g cm^{-3}.

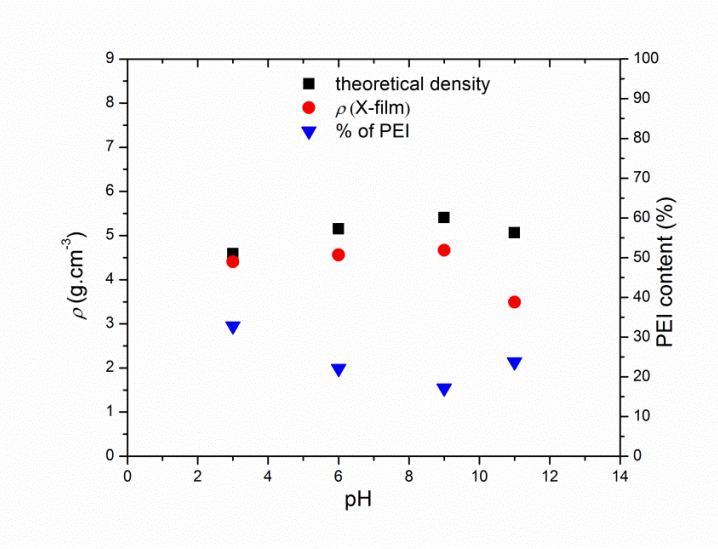

Figure 5: Variation of deposit density and %V of PEI as a function of pH

As a conclusion, the optimal pH condition is then pH=9 because, first the ζ is intermediate corresponding to an intermediate Debye length as it is already suggested by recent simulation [26], second, suspensions prepared at pH=9 results in the formation of deposits possessing high density. The EPD process at this pH showed homogeneous and bubble free deposits compared to those obtained at pH=3. As a result, the suspension conditions were fixed at pH=9 and the applied electric field and deposition time were varied.

3.2.3. Effect of the applied electric field

In order to study the effect of applied electric field (E), the deposition time was fixed at 120 minutes and E was varied between 1 and 5V cm^{-1}.

Since EPD is a kinetic phenomenon, the accumulation rate of the particles around the electrode could influence their packing behavior. As a result, the choice of the applied electric field could be critical for EPD affecting the morphology of the deposits [27]. High electric fields create turbulence around the deposition electrode due to the increased gas bubbles formation altering the morphology of deposit formed. Fig. 6 shows the top view SEM micrographs of deposits obtained. The size of the agglomerate increases with the increasing applied electric field varying between 50-200 nm for 2V cm^{-1}, ~500 nm for 3V cm^{-1} and 500-1000 nm for 4V cm^{-1} and

1000-2000 nm for 5V cm^{-1}. For 5V cm^{-1}, the obtained deposit has low adherence to the substrate due to the increased formation of gas bubbles, which prevents further deposition and causes the detachment of the formed deposit (see Fig. 6). As a conclusion, at lower electric fields as 2 V cm^{-1} deposits are formed from individual nanoparticles deposition, but with increasing the applied electric field nanoparticles are forced to migrate so fast without finding the right place to deposit and form close-packed structure.

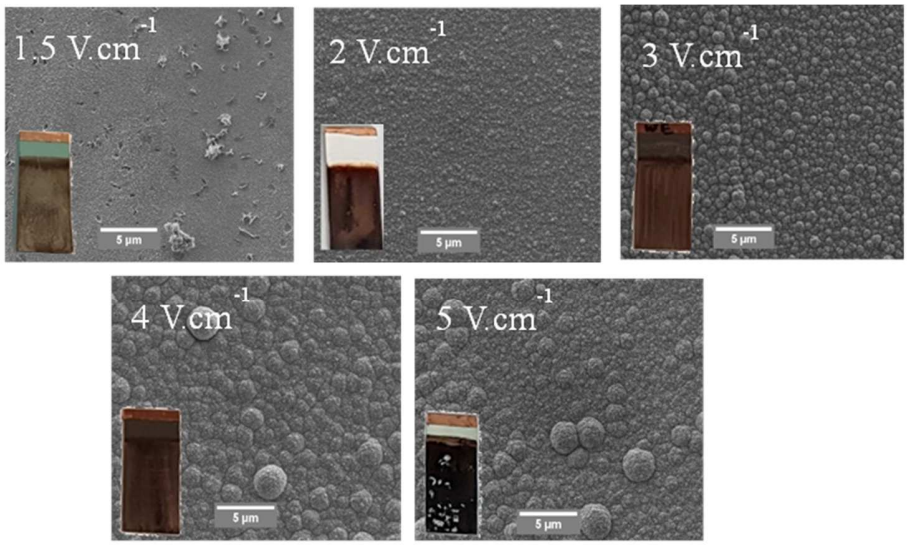

Figure 6: Top-view SEM micrographs of the obtained deposits for applied electric fields (1.5, 2, 3, 4, 5V cm^{-1}).

Fig. 7 shows the SEM micrographs of the obtained deposits in cross section view accompanied by the measured thickness and top-view (to analyze the morphology). The deposit thickness increases linearly with the applied electric field between E= 2 and 4V cm^{-1}, for higher electric field the thickness of the deposit saturated for a value of ~2600 nm. For E≤ 1V cm^{-1}, no deposit was observed at the cathode. The origin of this could be due to the fact that 1V cm^{-1} is not sufficient to form the first layer of CuO. For the slightly higher E=1.5V cm^{-1}, an irregular deposit of 108±11 nm thickness is deposited which also lies outside of the linear fit. This shows that an applied electric field E ≥ 2V cm^{-1} is required to allow the deposition phenomenon. While for E= 5 V cm^{-1} saturation is attained since as E increases, the deposition process is accelerated thus higher thickness is obtained in a shorter time increasing the resistance of the deposit preventing further deposition. As a result, 2V cm^{-1} is the optimum applied electric field in order to obtain a homogeneous and dense deposit possessing low surface roughness and high substrate adherence.

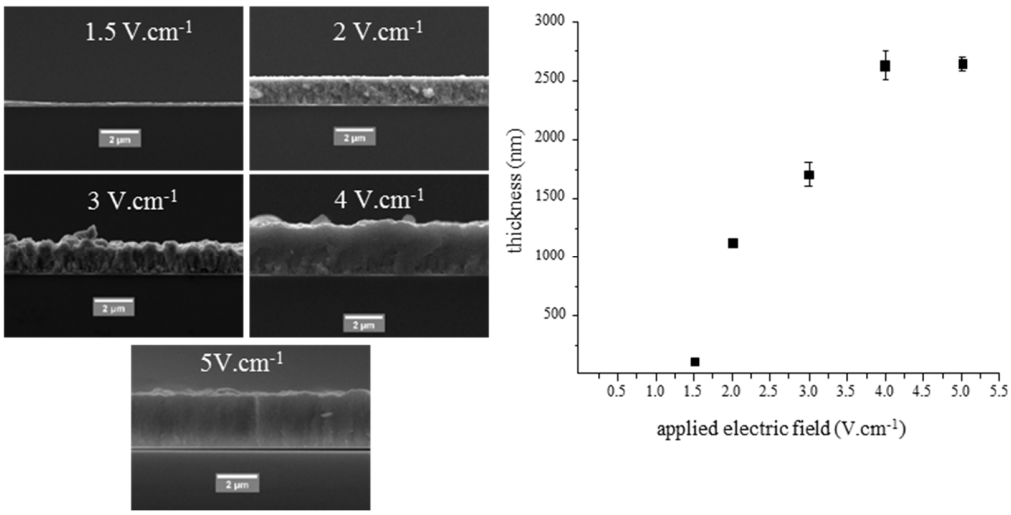

Figure 7: (right) SEM cross section micrographs of the effect of applied electric field. (left) Average measured thickness as a function of applied electric field (t=120 min).

3.2.4. Effect of the deposition time

To study of the evolution of the deposit thickness, as a function of deposition time, the applied electric field was fixed at 2V cm^{-1} and the deposition time was varied between 5, 10, 15, 30, 45, 60, 90, 120 and 180 min for the same suspension, Fig. 8 represents this evolution. In accordance with Hamaker equation, the deposit thickness increases linearly with deposition time between 5 and 30 min and then deviates from linearity after 30 min. However, the deviation from linearity is expected since the deposit formed with time creates a resisting layer that decreases the conductivity of the substrates preventing further linear deposition. Thus, for the linear part (5 and 30 mins), Hamaker equation could be used to calculate the effective density (ρ_e) of the deposit [27]. The ρ_e value is found to be 5.8g cm^{-3}, which is comparable with that obtained from X-film and TOC.

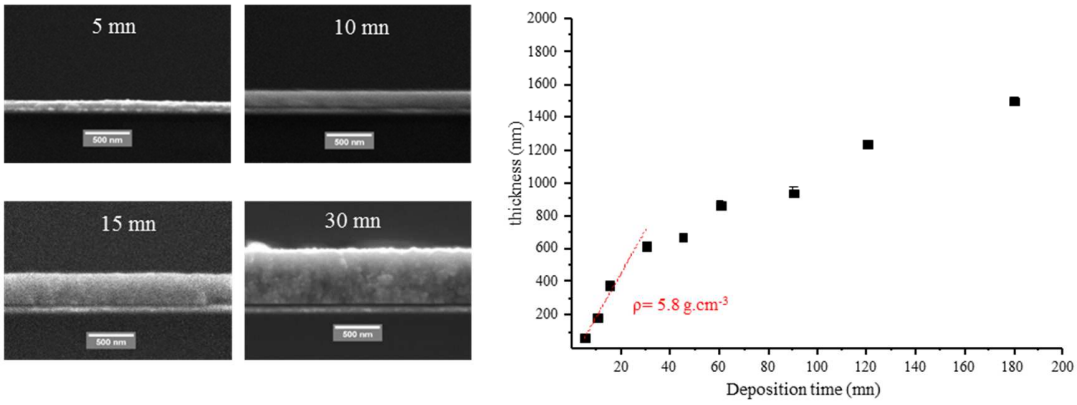

Figure 8: SEM cross section of the EPD deposits (right) and average measured thickness as a function of deposition time (5-180 min) (left).

3.2.5. Spectral efficiency

In Fig. 9, the calculated spectral features (α, ε, and η) of the EPD deposits obtained at different applied electric fields are represented. At 1V cm^{-1} nothing deposited at the electrode while increasing E slightly allowed the slight deposition of CuO and the α and ε values varied from that of the substrate. Increasing E to 2, 3, and 4V cm^{-1}, increased α and ε to 0.88-0.02, 0.86-0.01 and 0.8-0.03 respectively. As a result, the applied electric field increase doesn't enhance the α value, rather it is decreased for E = 2, 3 and 4V cm^{-1}. While for E= 5V cm^{-1}, α and ε attain the highest values of 0.95 and 0.44 resulting in a tandem absorber of low efficiency due to the high calculated ε. We point out that the deposits obtained at E=2V cm^{-1} present the highest efficiency of ~0.9.

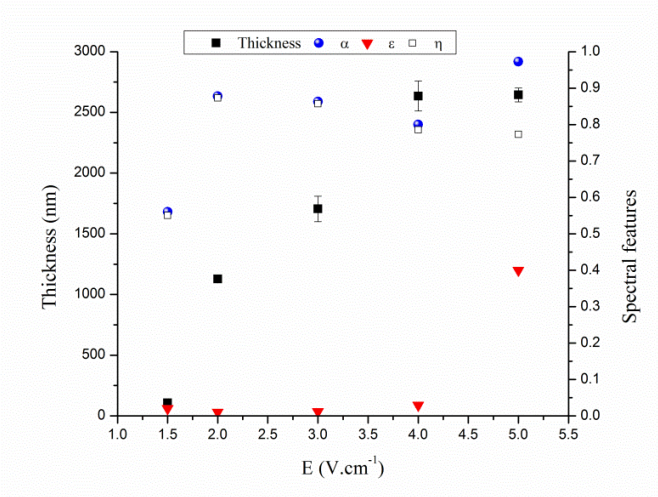

Figure 9: Measured thickness and spectral features of the obtained deposits at 1, 1.5, 2, 3, 4, 5V cm^{-1} for deposition time of 120 min.

Fig. 10 shows the average measured thickness (nm) and the calculated spectral efficiency as a function of deposition time (min). As expected, the deposition yield increases with deposition time. Upon EPD for 5 min, α value of the tandem absorber was 0.60. Then, with the deposition time increase, α value of 0.87 was reached for a deposition time of 120 min. On the other hand, the calculated emittance of CuO tandems varies between 0.01 and 0.09 for a deposition time varying between 5 and 120 min. Despite the formation of CuO thin film on the Pt Si wafer, the tandem absorbers still possess a low emittance and high absorptance. Thus, these tandem solar absorbers possess high efficiency (η). The highest efficiency of 0.84 is obtained for a deposition time of 120 mins and average measured thickness of 1240 ± 25 nm.

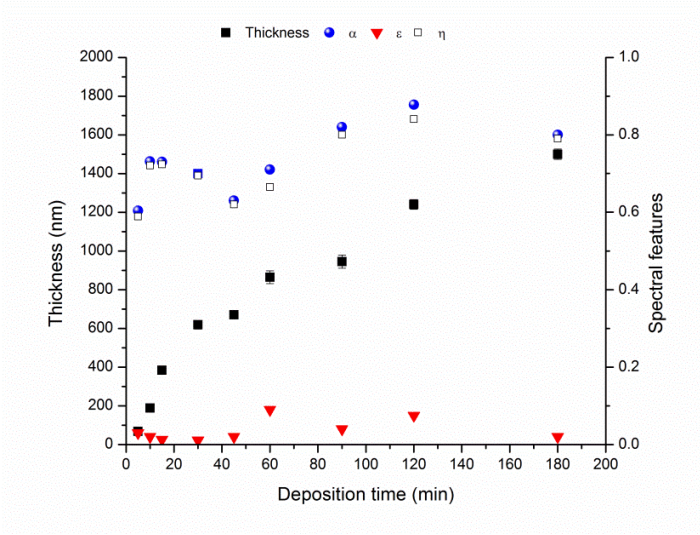

Figure 10: Calculated *α, ε* and *η and* measured deposit thickness as a function of deposition time (min).

4. Characterization of the deposit

In order to determine the composition of the deposit, we performed a conventional *Θ/2Θ* XRD scan, Grazing incidence XRD (GIXRD) and XPS on the CuO/PEI deposit on Pt Si wafer obtained at E=2V cm^{-1} and deposition time of 120 minutes from the suspensions prepared at pH=9.

4.1. X-ray diffraction study

Two intense peaks were obtained at 2Θ of 39.9 and 69.4. These peaks correspond to the peaks of the substrate. Upon deposition of CuO/PEI film, a slight shift in these peaks was observed and two new peaks appeared at 43.3° and 50.5°. These peaks were identified as Cu (111) and Cu (200) corresponding to face-centered cubic Copper (see Fig. 11).

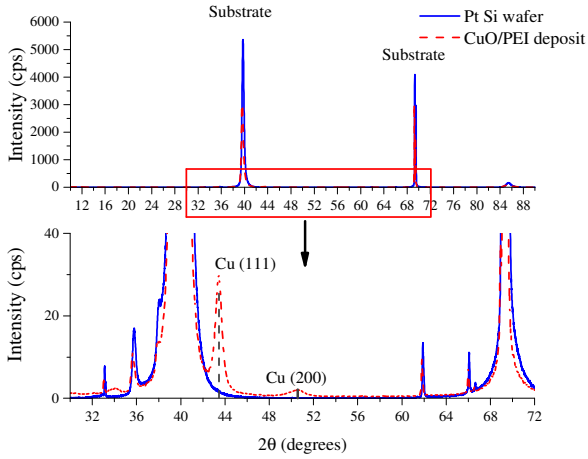

Figure 11: Θ/2Θ scan of XRD spectra of Pt Si wafer and CuO/PEI deposit.

Knowing that the main peaks corresponding to CuO, are located at 35.4° and 38.68° [4], could be masked by the substrate, we performed a 2Θ scan at a fixed grazing angle of incidence below the critical angle (Θ_c) of the substrate.

Then for the GIXRD analysis, incidence angle Θ_i is fixed to a value slightly above the critical angle of the material. In Fig. 12, the obtained GIXRD scan of the Pt Si wafer substrate shows a small hump at 39.9° corresponding to that of Pt and a strong peak at 69° corresponding to Si. Pt peak is observed more clearly when the Θ_i reaches 1°. While in Fig. 13, The scan of the deposit having a thickness of ~ 1500 nm is observed at Θ_i=0.4°, a small hump between 35° and 40° which could correspond to CuO or Cu_2O planes and an intense peak at 44° and 52° corresponding to Cu are also observed. Varying the angle of incidence has resulted in varying the intensity of the peak which increased as we penetrated the deposit.

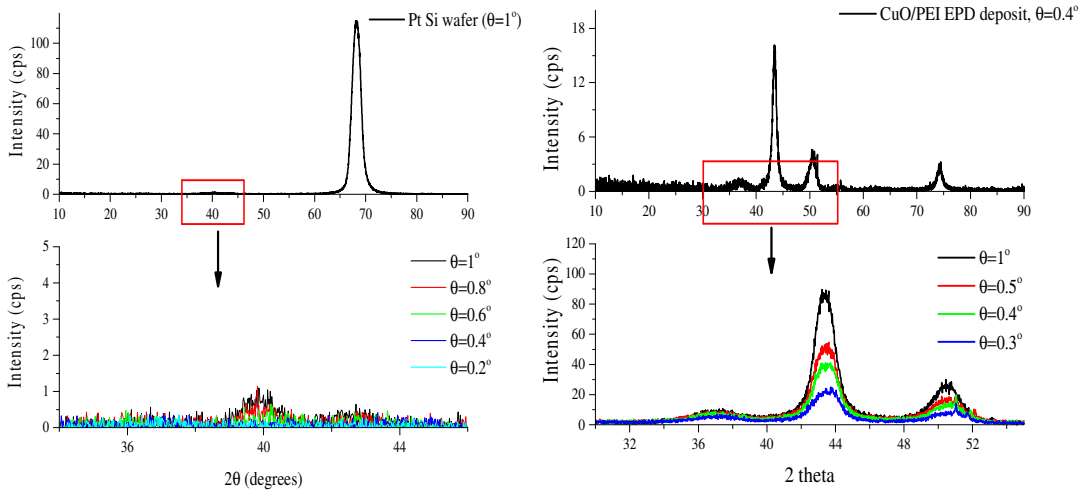

Figure 12 : GIXRD scans of (right) of Pt Si wafer and (left) of CuO/PEI EPD deposit (E=2 V.cm^{-1}, t=120 mins).

As a conclusion, the appearance of Cu(0) peaks in the XRD spectrum and the unresolved hump at ~36° suggests that part of the CuO NPs surface have been reduced. This mechanism is reported in literature by electrochemical reduction which could occur to bulk CuO nanoparticles or CuO films under cathodic applied electric field especially in alkaline conditions at 874 mV vs SCE [28] [29]. This reduction potential is equivalent to 913 mV for Ag/AgCl (3.5M KCl), which is inferior to the electric filed used for this study and then this scenario is plausible in our case.

4.2. X-ray photoelectron spectroscopy (XPS)

In order to identify the surface composition, the resulting CuO/PEI deposits are analyzed by XPS technique which analyzes the extreme surface (10-20 nm) (see Fig. 13). The peaks in the Cu2p scan corresponds to the core level $Cu2p_{1/2}$ and $Cu2p_{3/2}$ transitions of Cu. The binding energy (BE) at 932.5 eV corresponds to Cu(I) while the peak at 934.1 and shakeup satellites correspond to Cu(II). However, the peaks of Cu(I) and Cu (0) in Cu2p scan are very close and the difference is around 0.2 eV. Thus, a CuLMM scan is performed to differentiate these two peaks since the difference will be higher. The peak observed at 916.7 corresponds to Cu(I) and that at 918.5 corresponds to Cu(0). Moreover, the O1s peak at 530.5 eV corresponds to Oxygen bonded to Cu (MO) while that at 532 could correspond to C-O bonds (adventitious carbon). The peaks obtained in the C1s spectra corresponding to 284.9, 286.2, 288.6 eV, respectively proves the presence of adventitious carbon since the sample is dried in air. As a result, the data obtained from XPS, which analyzes only the extreme surface (20 nm) shows that the surface of CuO

nanoparticles is reduced into Cu_2O or Cu(0) due to the release of H_2 gas formed at the cathode as a result of electrolysis of water.

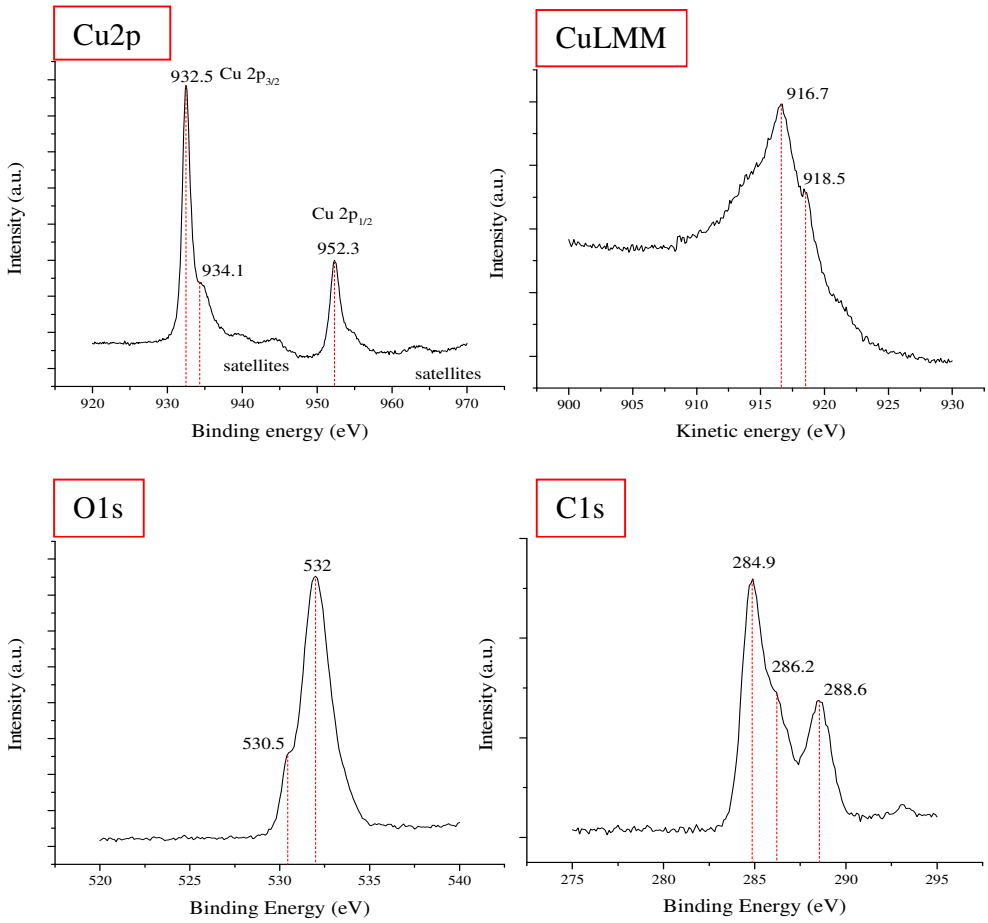

Figure 13: Cu2*p*, CuLMM, and O1s and C1s XPS spectra of CuO/PEI EPD deposit.

Combing the XRD, GIXRD and the XPS data we have concluded that CuO, Cu_2O and Cu coexist together in the deposit. This was also observed by the total reflectance spectra of the deposits, which showed a shift in the expected absorption edge of CuO. Compared to other reported work Cu has the least absorption in the UV-VIS-NIR region, while Cu_2O and CuO have higher absorption. Cu_2O has a better absorption in the UV-VIS while CuO absorbs better in the NIR region and a hybrid of CuO and Cu_2O results in an absorption and absorption edge intermediate between the two. As a mechanism we propose that CuO is reduced by electrochemical reduction at the cathode forming a hybrid composite of Cu, CuO, and Cu_2O [29].

Conclusion

A cathodic EPD of CuO nanoparticles (size of 25±5 nm) stabilized by PEI has been yield a dense and crack-free coating displaying high optical efficiency. For this, the EPD processing parameters (applied electric field, deposition time) are adjusted in order to control the structure (density, roughness, thickness) and consequently the optical efficiency of the deposit. The colloidal route offers the advantage of the formation of the CuO film from a bottom-up approach controlling the features of the film. Best selective low temperature tandem materials, having a high density (≈5.9g cm^{-3} for pH=9) and obtained during 120 mins at E=2V cm^{-1}, provide an efficiency closed to 0.9 which is prominent to be used as solar selective absorbers.

Acknowledgement

The authors would like to thank the University of Montpellier and the Lebanese National council for Scientific research (CNRS-L) for the co-joint funding of the project and the attribution of PhD's fellowship. The authors are grateful to Alban Jonchère (ICSM) for his help during the reflectance measurements.

References

[1] D. Katzen, E. Levy, Y. Mastai, Thin films of silica-carbon nanocomposites for selective solar absorbers, Applied Surface Science, 248 (2005) 514-517.
[2] A. Amri, Z.T. Jiang, T. Pryor, C.Y. Yin, S. Djordjevic, Developments in the synthesis of flat plate solar selective absorber materials via sol-gel methods: A review, Renewable & Sustainable Energy Reviews, 36 (2014) 316-328.
[3] T. Karlsson, A. Roos, Optical properties and spectral selectivity of copper oxide on stainless steel Solar Energy Materials, 10 (1984) 105-119.
[4] T. Maruyama, Copper oxide thin films prepared by chemical vapor deposition from copper dipivaloylmethanate, Solar Energy Materials and Solar Cells, 56 (1998) 85-92.
[5] P. Richharia, K.L. Chopra, M.C. Bhatnagar, Surface analysis of a black copper selective coating Solar Energy Materials, 23 (1991) 93-109.
[6] A.O. Musa, T. Akomolafe, M.J. Carter, Production of cuprous oxide, a solar cell material, by thermal oxidation and a study of its physical and electrical properties, Solar Energy Materials and Solar Cells, 51 (1998) 305-316.
[7] A.H. Jayatissa, K. Guo, A.C. Jayasuriya, Fabrication of cuprous and cupric oxide thin films by heat treatment, Applied Surface Science, 255 (2009) 9474-9479.
[8] X.D. Xiao, L. Miao, G. Xu, L.M. Lu, Z.M. Su, N. Wang, S. Tanemura, A facile process to prepare copper oxide thin films as solar selective absorbers, Applied Surface Science, 257 (2011) 10729-10736.
[9] A. Marquez, G. Blanco, M.E.F. de Rapp, D.G. Lamas, R. Tarulla, Properties of cupric oxide coatings prepared by cathodic arc deposition, Surface & Coatings Technology, 187 (2004) 154-160.
[10] T.S. Sathiaraj, Solar selective properties of copper-aluminium composite films, Indian Journal of Pure & Applied Physics, 45 (2007) 613-617.

[11] C.G. Granqvist, Solar energy materials, Advanced Materials, 15 (2003) 1789-1803.
[12] C.M. Lampert, Coatings for enhanced photothermal energy collection Solar Energy Materials, 1 (1979) 319-341.
[13] L. Fedele, L. Colla, S. Bobbo, S. Barison, F. Agresti, Experimental stability analysis of different water-based nanofluids, Nanoscale Research Letters, 6 (2011).
[14] M. Guedes, J.M.F. Ferreira, A.C. Ferro, A study on the aqueous dispersion mechanism of CuO powders using Tiron, Journal of Colloid and Interface Science, 330 (2009) 119-124.
[15] S. Mallakpour, M. Dinari, E. Azadi, Poly(vinyl alcohol) Chains Grafted onto the Surface of Copper Oxide Nanoparticles: Application in Synthesis and Characterization of Novel Optically Active and Thermally Stable Nanocomposites Based on Poly(amide-imide) Containing N-trimellitylimido-L-valine Linkage, International Journal of Polymer Analysis and Characterization, 20 (2015) 82-97.
[16] D.P. Kulkarni, D.K. Das, S.L. Patil, Effect of temperature on rheological properties of copper oxide nanoparticles dispersed in propylene glycol and water mixture, Journal of Nanoscience and Nanotechnology, 7 (2007) 2318-2322.
[17] R. Laucournet, C. Pagnoux, T. Chartier, J.F. Baumard, Coagulation method of aqueous concentrated alumina suspensions by thermal decomposition of hydroxyaluminum diacetate, Journal of the American Ceramic Society, 83 (2000) 2661-2667.
[18] C. Pagnoux, Suspension systems for coagulation processing, Journal of Ceramic Processing Research, 3 (2002) 10-14.
[19] M. Mishra, Y. Sakka, T. Uchikoshi, L. Besra, pH localization: a case study during electrophoretic deposition of ternary MAX phase carbide-Ti3SiC2, Journal of the Ceramic Society of Japan, 121 (2013) 348-354.
[20] C. Mendoza, Z. Gonzalez, Y. Castro, E. Gordo, B. Ferrari, Improvement of TiN nanoparticles EPD inducing steric stabilization in non-aqueous suspensions, Journal of the European Ceramic Society, 36 (2016) 307-317.
[21] M. Zarbov, I. Schuster, L. Gal-Or, Methodology for selection of charging agents for electrophoretic deposition of ceramic particles, Journal of Materials Science, 39 (2004) 813-817.
[22] M. Verde, M. Peiteado, A.C. Caballero, M. Villegas, B. Ferrari, Electrophoretic Deposition of Transparent ZnO Thin Films from Highly Stabilized Colloidal Suspensions, Journal of Colloid and Interface Science, 373 (2012) 27-33.
[23] T. Wen, F. Qu, N.B. Li, H.Q. Luo, A facile, sensitive, and rapid spectrophotometric method for copper(II) ion detection in aqueous media using polyethyleneimine, Arabian Journal of Chemistry, 10 (2017) S1680-S1685.
[24] J. Jia, A.H. Wu, S.J. Luan, Spectrometry recognition of polyethyleneimine towards heavy metal ions, Colloids and Surfaces a-Physicochemical and Engineering Aspects, 449 (2014) 1-7.
[25] M. Ammam, Electrophoretic deposition under modulated electric fields: a review, Rsc Advances, 2 (2012) 7633-7646.
[26] B. Giera, L.A. Zepeda-Ruiz, A.J. Pascall, T.H. Weisgraber, Mesoscale Particle-Based Model of Electrophoretic Deposition, Langmuir, 33 (2017) 652-661.
[27] S. Shehayeb, X. Deschanels, I. Karame, L. Ghannam, G. Toquer, Spectrally selective coatings obtained from electrophoretic deposition of CuO nanoparticles, Surface & Coatings Technology, 322 (2017) 38-45.
[28] W.K. Han, J.W. Choi, G.H. Hwang, S.J. Hong, J.S. Lee, S.G. Kang, Fabrication of Cu nano particles by direct electrochemical reduction from CuO nano particles, Applied Surface Science, 252 (2006) 2832-2838.
[29] Y. Wan, Y.D. Zhang, X.L. Wang, Q. Wang, Electrochemical formation and reduction of copper oxide nanostructures in alkaline media, Electrochemistry Communications, 36 (2013) 99-102.